

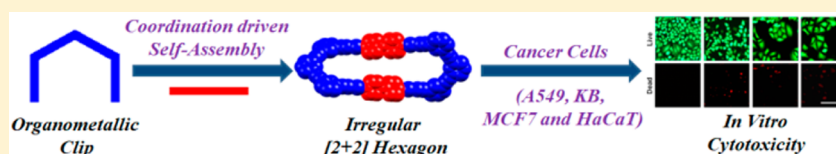
Coordination-Driven Self-Assembly of Ionic Irregular Hexagonal Metallamacrocycles via an Organometallic Clip and Their Cytotoxicity Potency

Sourav Bhowmick,[†] Achintya Jana,[†] Khushwant Singh,[†] Prerak Gupta,[‡] Ankit Gangrade,[‡] Biman B. Mandal,^{*,‡,†} and Neeladri Das^{*,†,†}

[†]Department of Chemistry, Indian Institute of Technology Patna, Bihta 801103, Bihar, India

[‡]Department of Biosciences and Bioengineering, Indian Institute of Technology Guwahati, Guwahati 781039, Assam, India

Supporting Information



ABSTRACT: Two new irregular hexagons (6 and 7) were synthesized from a pyrazine motif containing an organometallic acceptor clip [bearing platinum(II) centers] and different neutral donor ligands (4,4'-bipyridine or pyrazine) using a coordination-driven self-assembly protocol. The two-dimensional supramolecules were characterized by multinuclear NMR, mass spectrometry, and elemental analyses. Additionally, one of the macrocycles (6) was characterized by single-crystal X-ray analyses. Macrocycles are unique examples of [2 + 2] self-assembled ensembles that are hexagonal but irregular in shape. These hexagon frameworks require the assembly of only four tectons/subunits. The cytotoxicity of platinum(II)-based macrocycles was studied using various cell lines such as A549 (human lung carcinoma), KB (human oral cancer), MCF7 (human breast cancer), and HaCaT (human skin keratinocyte) cell lines, and the results were compared with those of cisplatin. The smaller macrocycle (7) exhibited a higher cytotoxic effect against all cell types, and its sensitivity was found to be comparable with that of cisplatin for A549 and MCF7 cells. Cell cycle analysis and live propidium iodide staining suggest that the macrocycles 6 and 7 induced a loss of membrane integrity that ultimately might lead to necrotic cell death.

INTRODUCTION

The strategy of utilizing metal–ligand coordination to yield discrete molecular species has emerged as a well-established protocol in supramolecular chemistry.¹ Herein, the term “ensemble” has been frequently used to describe a molecular entity that is usually in nanoscale dimensions.² The phrase “molecular subunit” is used to describe organic or metal-bearing (organometallic) smaller molecules that bind with one another via coordination bonds in a chemical reaction that is popularly referred to as a “self-assembly” process.³ The phrase “self-assembly” refers to a chemical reaction that utilizes the molecular information present in the “molecular subunit” to yield a molecular “ensemble” of predefined shape and size.^{1a,b,4} These reactions do not require any human intervention because the information (such as the bite angle) contained in the molecular subunit determines the geometrical shape of the resultant supramolecular framework.^{1a,b,4a–c}

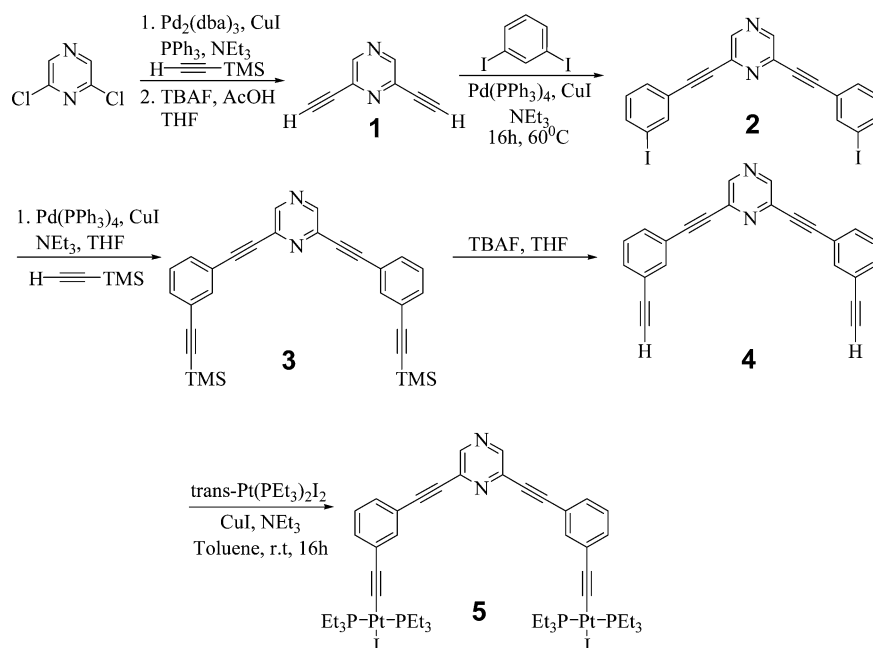
It is well-known that inorganic complexes such as cisplatin, carboplatin, and others are widely used drugs for the treatment of various types of cancers.⁵ However, there are certain limitations of cisplatin and related complexes that include, but are not limited, to high toxicity, undesired side effects, shorter half-life, and a lower spectrum of effectiveness as well as a tendency of tumor cells to acquire resistance.⁶ This has

motivated research interest in developing organometallic complexes as drugs for such medical treatment and investigating their potential in anticancer activity.⁷ Organometallic complexes have been reported to be more potent than their nonorganometallic/inorganic counterparts because the former are more inert kinetically relative to the latter.^{7a,8} In recent years, the effectiveness of organometallic compounds as potential anticancer drugs has been documented in a review article.⁹ As far as the metal center is concerned, the use of ruthenium,¹⁰ palladium,¹¹ and platinum¹² in anticancer organometallic metallodrugs is more common. In this context, discrete supramolecular species bearing multiple metal centers are new additions in the library of compounds with anticancer activity and coordination-driven self-assembly is a facile synthetic strategy for the design of such discrete frameworks. Two-dimensional metal-containing macrocycles (metallamacrocycles) and three-dimensional metallacages have been reported to have biomedical applications.⁹ Their interaction with biomolecular species such as DNA or cancerous cells has been studied in the past.¹³ Among the different types of self-

Special Issue: Self-Assembled Cages and Macrocycles

Received: June 19, 2017

Scheme 1. Synthesis of the Pyrazine-Based Organoplatinum Clip 5



assembled architectures whose biological properties have been studied, a majority of these ensembles have ruthenium(III) as the metal center.¹⁴ Literature reports describing the study of the anticancer activity of discrete self-assembled ensembles (metallomacrocycles or metallocages) containing other metals such as palladium(II) and platinum(II) are relatively less common, although cisplatin contains platinum(II).

Herein, in a continuation of our research interest to develop new metallosupramolecular architectures, we report the design of a new organometallic diplatinum molecular “clip” as an acceptor tecton that was used as a building block for the synthesis of two nanodimensional molecular hexagonal-shaped macrocycles. Subsequently, for the first time, cytotoxic efficacies of platinum(II)-based macrocycles were studied (using these macrocycles) against four different cancer cell lines, and the results obtained were compared with those of cisplatin.

RESULT AND DISCUSSION

Synthesis and Characterization of the Pyrazine-Based Organometallic Clip 5. A new pyrazine-based organometallic clip **5**, has been synthesized via multistep reactions using commercially available 2,6-dichloropyrazine (Scheme 1) as the synthon. First, 2,6-bis[(trimethylsilyl)ethynyl]pyrazine was synthesized using a well-known Sonogashira cross-coupling reaction, followed by deprotection of the trimethylsilyl group, which yielded 2,6-diethynylpyrazine (**1**). Subsequently, using a coupling reaction between **1** and 1,3-diiodobenzene in the presence of cuprous iodide/palladium(0) catalysts and triethylamine (base) at 60 °C for 16 h, 2,6-bis[(3-iodophenyl)ethynyl]pyrazine (**2**) was obtained in reasonably high yields (>80%). In subsequent steps, 2,6-bis[(3-ethynylphenyl)ethynyl]pyrazine (**4**) was synthesized by the cross-coupling reaction of **2** with (trimethylsilyl)acetylene in tetrahydrofuran (THF) as the solvent and using the same catalyst and base as those utilized in a previous step. Subsequently, deprotection with tetra-*n*-butylammonium fluoride (TBAF; THF as the solvent) yielded the desired intermediate (**4**). The pyrazine-based organometallic clip **5** was finally synthesized by reacting **4**

with 2 equiv of *trans*-PtI₂(PEt₃)₂ in the presence of CuI (catalyst), triethylamine (base), and toluene (solvent) at room temperature for 16 h (Scheme 1). **5** is a new organometallic clip that was obtained in 68% yield as a yellowish semisolid and is stable in air/moisture with high solubility in common organic solvents. All new molecules (**2–5**) were characterized by Fourier transform infrared (FT-IR) and NMR (¹H and ¹³C) spectroscopy, mass spectrometry, and elemental analyses. In addition, the molecular structure of **4** was confirmed by single-crystal X-ray analysis. In FT-IR spectra of **2** and **4**, the presence of strong bands at 2218 and 2212 cm⁻¹ [$\nu(\text{C}\equiv\text{C}_{\text{str.}}$)], respectively, indicates the presence of an internal ethynyl functional group in these products. In ¹H NMR spectra of **2** and **4** (Supporting Information S2 and S3), the sharp singlets at 8.65 and 8.66 ppm, respectively, were assigned to the aromatic protons of the pyrazine ring present in these molecules. Four sets of signals were observed in the ¹H NMR spectra because of four different kinds of chemically inequivalent protons in **2** and **4** (Supporting Information S2 and S3). Additionally, in the case of **4**, the sharp singlet at 3.12 ppm was due to an ethynyl proton. All of the characteristic peaks corresponding to the pyrazine, phenyl, and ethynyl units of both **2** and **4** were observed in the ¹³C{¹H} NMR spectrum (Supporting Information S2 and S3). The new pyrazine-based organometallic clip **5** has been characterized by FT-IR, multinuclear NMR (¹H, ¹³C, and ³¹P) spectroscopy, mass spectrometry, and elemental analyses. In the FT-IR spectrum of **5**, the presence of two different ethynyl functional groups was evident because of the presence of intense peaks at 2210 and 2113 cm⁻¹. In the ¹H NMR spectrum of **5** (Supporting Information S4), a sharp singlet at 8.64 ppm corresponds to the aromatic protons of pyrazine. Four sets of signals were observed in the ¹H NMR because of the four different chemically inequivalent protons of the phenyl ring (Supporting Information S4). As expected, the methylene and methyl protons of the PEt₃ groups appear as multiplets in the ranges of 2.26–2.19 and 1.22–1.14 ppm, respectively. In the ³¹P NMR spectrum of **5** (Supporting Information S4), one sharp singlet observed at 8.87 ppm,

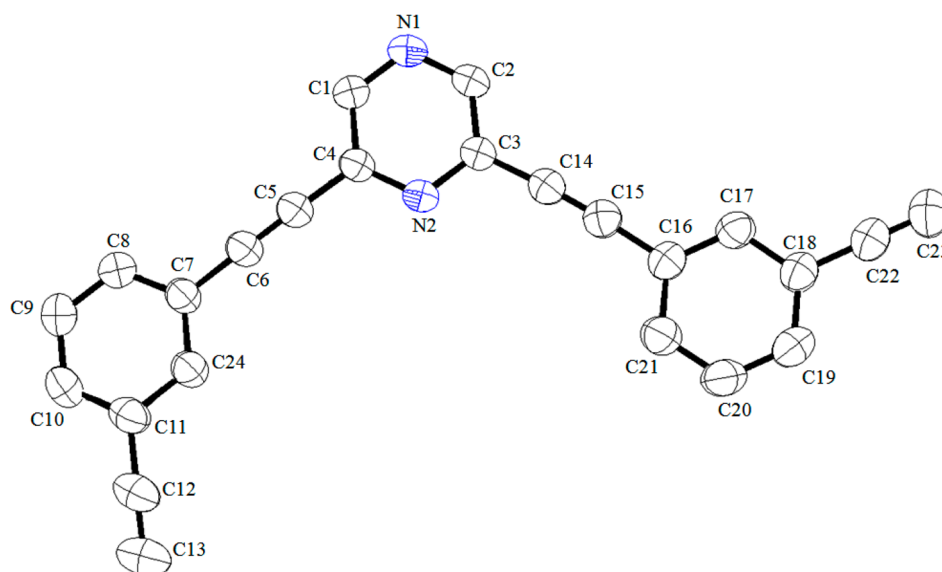
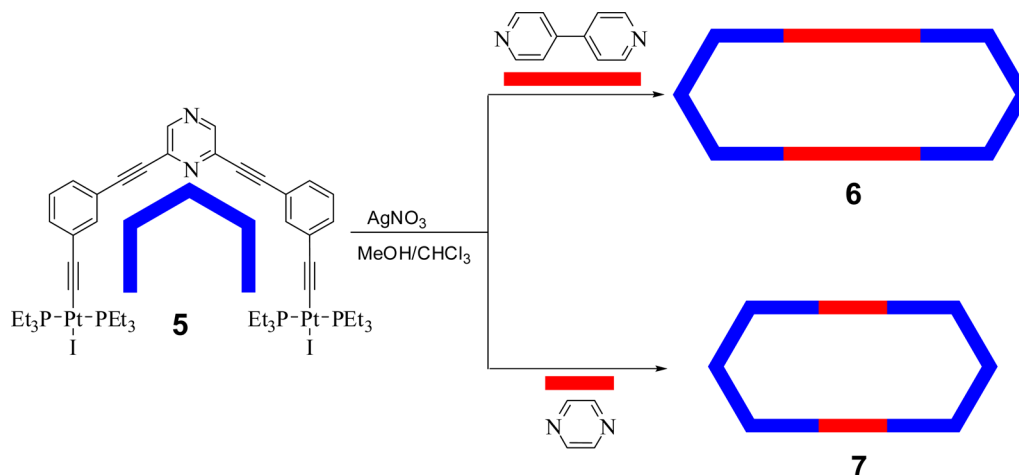


Figure 1. ORTEP representation of 4. Thermal ellipsoids were drawn at the 50% probability level. Hydrogen atoms were omitted for clarity.

Scheme 2. Design of Irregular Hexagonal Macrocycles 6 and 7



accompanied by concomitant ^{195}Pt satellites ($^1J_{\text{Pt}} = 1147 \text{ Hz}$), suggests that all phosphorus nuclei attached to platinum(II) centers are chemically equivalent in 5.

X-ray Crystallographic Analysis of 4. Single crystals of 4 (suitable for X-ray diffraction) were obtained by the slow evaporation of its dichloromethane solution at ambient temperature. Compound 4 crystallizes in the triclinic space group $P\bar{1}$. Crystal structure analysis reveals no unusual bond lengths or angles within the molecule. The molecular structure with the numbering scheme is shown in Figure 1. Both pendent 1,3-diethynylbenzene moieties are in the same plane as the central pyrazine ring. However, the orientations of the two terminal ethynyl moieties of 4 are trans to each other. Detailed crystallographic analysis revealed that both nitrogen atoms (N1 and N2) of the pyrazine ring of a given molecule 4 have hydrogen-bonding interactions with the neighboring molecule. The hydrogen-bond parameters found in 4 are tabulated in Supporting Information S8. The intermolecular hydrogen-bonding interactions are shown in Supporting Information S8.

Application of the Organometallic Clip 5 as a Molecular Tecton for the Self-Assembly of Irregular Hexagonal Macrocycles. Continuing our research interest in

constructing discrete metal-containing macrocyclic species derived from pyrazine molecules, we describe the use of a new organometallic tecton (5) as a building block to yield two hexagonal ensembles via a coordination-driven self-assembly reaction. Usually the construction of discrete hexagonal macrocyclic species requires the self-assembly of a relatively larger number of donor and acceptor units. However, our strategy involves the utilization of a relatively lesser number of donor/acceptor units [2 + 2] to obtain a hexagonal entity that otherwise requires a [6 + 6] or [3 + 3] combination of complementary tectons. Herein, we have synthesized two hexagonal-shaped macrocycles in which two ditopic acceptor tectons self-assemble with two linear ditopic donor tectons to yield a [2 + 2] assembly. The diplatinum acceptor organometallic clip (5) was first reacted with 2 equiv of silver nitrate, and the dinitrate derivative (generated in situ) was reacted with a suitable linear ditopic donor tecton (4,4'-bipyridine or pyrazine) in a 1:1 stoichiometric ratio (Scheme 2). This resulted in the exclusive formation of the hexagonal macrocycles 6 and 7 via a [2 + 2] coordination-driven self-assembly (Scheme 2). The crude product thus obtained (after solvent evaporation) was washed with *n*-pentane and subsequently

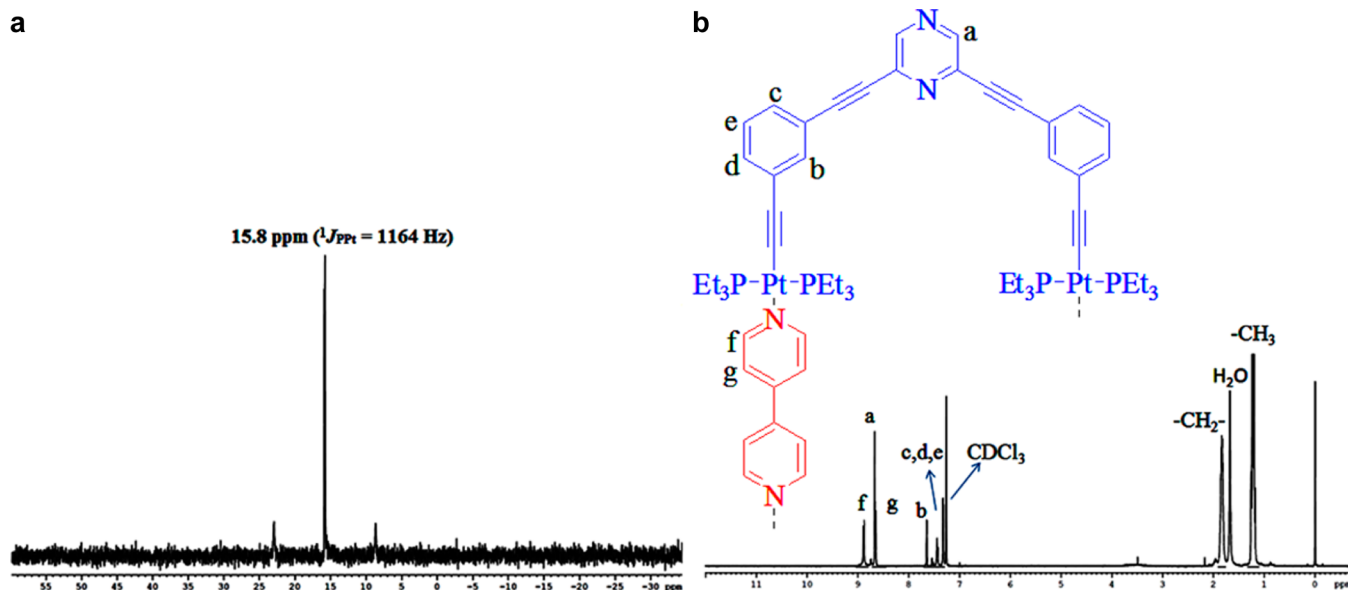


Figure 2. (a) $^{31}\text{P}\{^1\text{H}\}$ and (b) ^1H NMR spectra of the macrocycle **6**.

recrystallized from chloroform/methanol to obtain the desired macrocycles as a yellowish microcrystalline solid in reasonable yield (>90%). In both cases, the product obtained was soluble in organic solvents.

The formation of macrocycles was subsequently confirmed by analytical techniques such as multinuclear NMR spectroscopy, electrospray ionization time-of-flight mass spectrometry (ESI-TOF-MS), and elemental analyses. In addition, the molecular structure of **6** was unambiguously determined by X-ray crystallography analysis. $^{31}\text{P}\{^1\text{H}\}$ NMR analyses of **6** and **7** are consistent with the formation of a single, highly symmetrical species due to the appearance of sharp singlets respectively at 15.88 and 20.13 ppm with concomitant ^{195}Pt satellite peaks (**6**, $^1J_{\text{PPt}} = 1164$ Hz; **7**, $^1J_{\text{PPt}} = 1237$ Hz). These peaks are shifted relative to that of **5** ($\Delta\delta = 7.29$ and 11.54 ppm) for products **6** and **7**, respectively (Figure 2 and Supporting Information S5–S8). The ^1H NMR spectra of macrocycles **6** and **7** also confirmed the formation of pure and highly symmetrical structures. A significant shift in the position of the peaks corresponding to the reacting donor and acceptor tectons was observed upon coordination. The ^1H NMR spectra of products **6** and **7** clearly suggested the incorporation of a donor tecton (4,4'-bipyridine in the case of **6** and pyrazine in the case of **7**) and an acceptor pyrazine-based clip (**5**) in the respective final product (Figure 2 and Supporting Information S5–S8). In ^1H NMR spectrum of **6**, two doublet peaks appeared at 8.89–8.88 and 8.66–8.65 ppm, and these were assigned to the protons of the 4,4'-bipyridine units. The signals at 8.67, 7.64, 7.45–7.44, and 7.32–7.31 ppm correspond to the pyrazine and phenyl protons of the acceptor unit (Figure 2) in **6**. The presence of the PEt_3 groups attached to the platinum(II) centers was evident from the signals due to the ethyl protons in the ^1H NMR spectrum in the range of 1.85–1.17 ppm (Figure 2), and this confirmed the incorporation of the acceptor tecton in this self-assembled product (**6**). Similarly, in the case of **7**, all proton signals in ^1H NMR were assigned correctly (Supporting Information S7).

The [2 + 2] self-assembly involving two units of donor and acceptor tectons were confirmed by ESI-MS analysis. The ESI-TOF-MS spectrum of **6** (Figure 3) shows signals due the

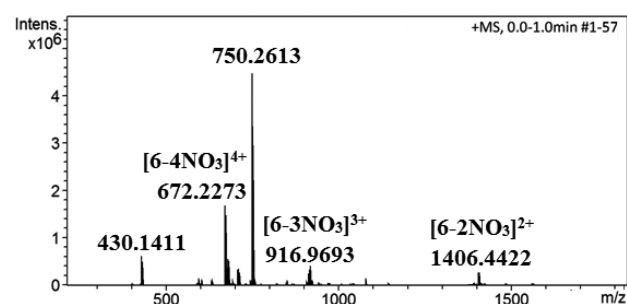


Figure 3. ESI-MS data of the macrocycle **6**.

consecutive loss of nitrate counteranions from the expected [2 + 2] macrocycle at m/z 1406.43 ($[\text{6} - 2\text{NO}_3^-]^{2+}$), 916.95 ($[\text{6} - 3\text{NO}_3^-]^{3+}$), and 672.22 ($[\text{6} - 4\text{NO}_3^-]^{4+}$). Similarly, for compound **7**, peaks were observed at m/z 1330.42 ($[\text{7} - 2\text{NO}_3^-]^{2+}$), 866.28 ($[\text{7} - 3\text{NO}_3^-]^{3+}$), and 634.21 ($[\text{7} - 4\text{NO}_3^-]^{4+}$) in the ESI-TOF-MS spectrum, confirming the formation of the [2 + 2] macrocyclic architecture (Supporting Information S9).

X-ray Crystallographic Analysis of 6. There are a handful reports in the literature where the crystal structures of ionic platinum metallacycles [synthesized from platinum(II) acceptor tectons and bipyridine donors] are reported.¹⁵ After repeated trials, X-ray-quality single crystals of **6** were obtained by the slow vapor diffusion of diethyl ether into its solution in a solvent mixture ($\text{CH}_2\text{Cl}_2/\text{CH}_3\text{OH}$) at room temperature. Figure 4 shows the molecular structure of **6**, which crystallizes in the triclinic space group $P\bar{1}$. The ball-and-stick presentation of the ionic irregular hexagon **6** is shown in Figure 4. The molecular structure of **6** consists of two molecular clips that are bridged by two 4,4'-bipyridine units through nitrogen atoms and forms a highly twisted Pt_4 molecular irregular hexagon, as shown in Figure 4B. The geometry around each platinum is close to square-planar, with the cis angles in the range of 86–95° (Supporting Information S9 and S10). There are two nitrate anions that are crystallographically disordered. They are situated outside the hexagon pockets of **6**. The important crystallographic parameters for **6** are presented in Supporting

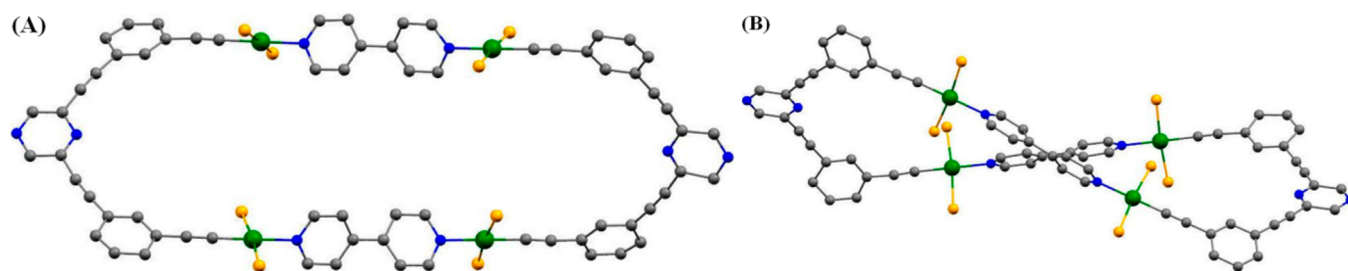


Figure 4. (A) Ball-and-stick representation of **6**. (B) Ball-and-stick representation illustrating the inherent twist present in the molecular irregular hexagon **6**. The ethyl groups attached to the phosphorus atoms and all counteranions (NO_3^-) are omitted for clarity.

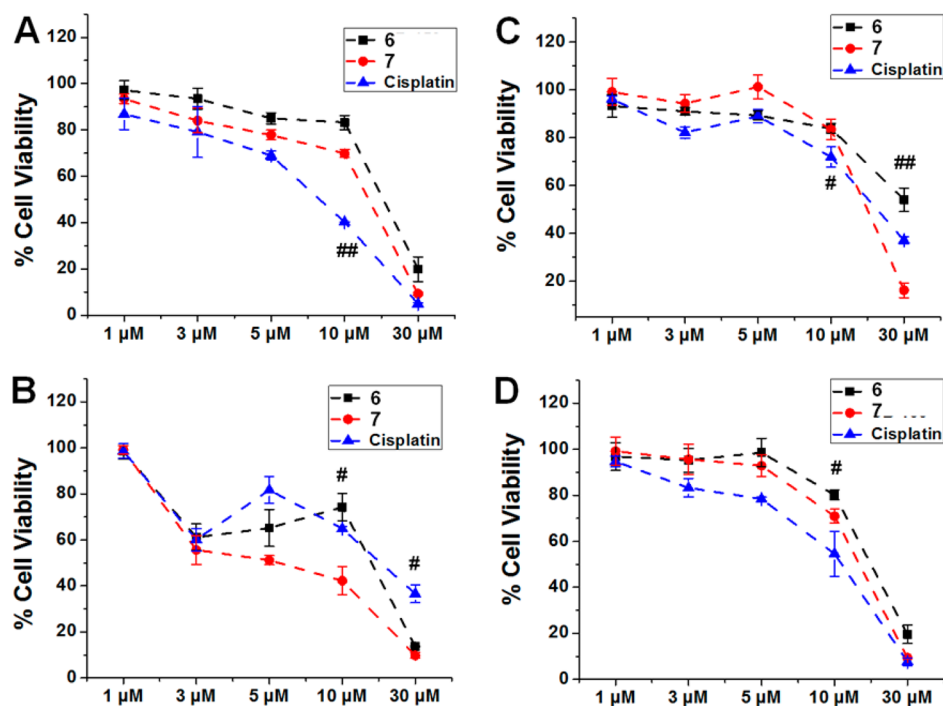


Figure 5. In vitro cytotoxicity of synthesized compounds (**6** and **7**) and cisplatin against (A) A549, (B) MCF7, (C) KB, and (D) HaCaT cells after 48 h of treatment as determined by MTT assay. Data points represent mean \pm standard deviation for at least three independent experiments (#, $p < 0.05$; ##, $p < 0.01$).

Information S9. The distance between Pt(01) and Pt(03) is 8.3414 (0.0017) Å, and that between Pt(02) and Pt(04) is 8.3937 (0.0017) Å. The length of **6** is 29.959 Å, as defined by the distance between the centroids of the pyrazine rings of the molecular clip. The distortion in the hexagon shape of the metallacycle **6** is probably due to the steric effect exerted by the adjacent triethylphosphine ligands. This is more clearly evident from the CPK representation (space-filled model of **6** in Supporting Information S11); it appears that this repulsive interaction has been partially relieved in the entire molecule by incorporating a dihedral twist ($\Phi \approx 20.6^\circ$), and this is possible because of the free rotation of the terminal ethynylbenzene moieties of the molecular clip **6**.

Overall, the stoichiometry and composition of the [2 + 2] macrocycle, as predicted by NMR spectroscopy and mass spectrometry, were confirmed by X-ray analysis of **6**.

In Vitro Cytotoxicity and Determination of the IC_{50} Value. The cytotoxic activity of both compounds were tested against four cell lines, viz., A549 (human lung carcinoma cell line), KB (human oral cancer cell line), MCF7 (human breast cancer cell line), and HaCaT (human skin keratinocyte cell line) and compared with that of cisplatin. **7** was found to be

more toxic for each cell line and exhibited a lesser IC_{50} value compared to **6**. A five-point dose-dependent curve was plotted for each cell line (Figure 5), and the IC_{50} concentration was calculated for both compounds (Table 1). The IC_{50}

Table 1. IC_{50} Concentration (μM) of Compounds against Different Cancer Cells

	$\text{IC}_{50}/\mu\text{M}$			
	A549 cells	MCF7 cells	KB cells	HaCaT cells
cisplatin	25.0 ± 0.3	20.0 ± 0.3	08.0 ± 0.4	12.0 ± 0.3
6	>30.0	17.0 ± 0.3	20.0 ± 0.1	20.0 ± 0.1
7	20.0 ± 0.2	05.0 ± 0.2	16.0 ± 0.4	16.0 ± 0.5

concentration is defined as the compound concentration at which 50% of the cells were viable. Both compounds and cisplatin showed concentration-dependent cytotoxic effects. At lower concentrations ($\sim 1 \mu\text{M}$), no cytotoxic effect was observed for any compound. A549 cells were found to be least sensitive for cisplatin (IC_{50} value of $25.0 \pm 0.3 \mu\text{M}$) and **6** (IC_{50} value of $>30.0 \mu\text{M}$).

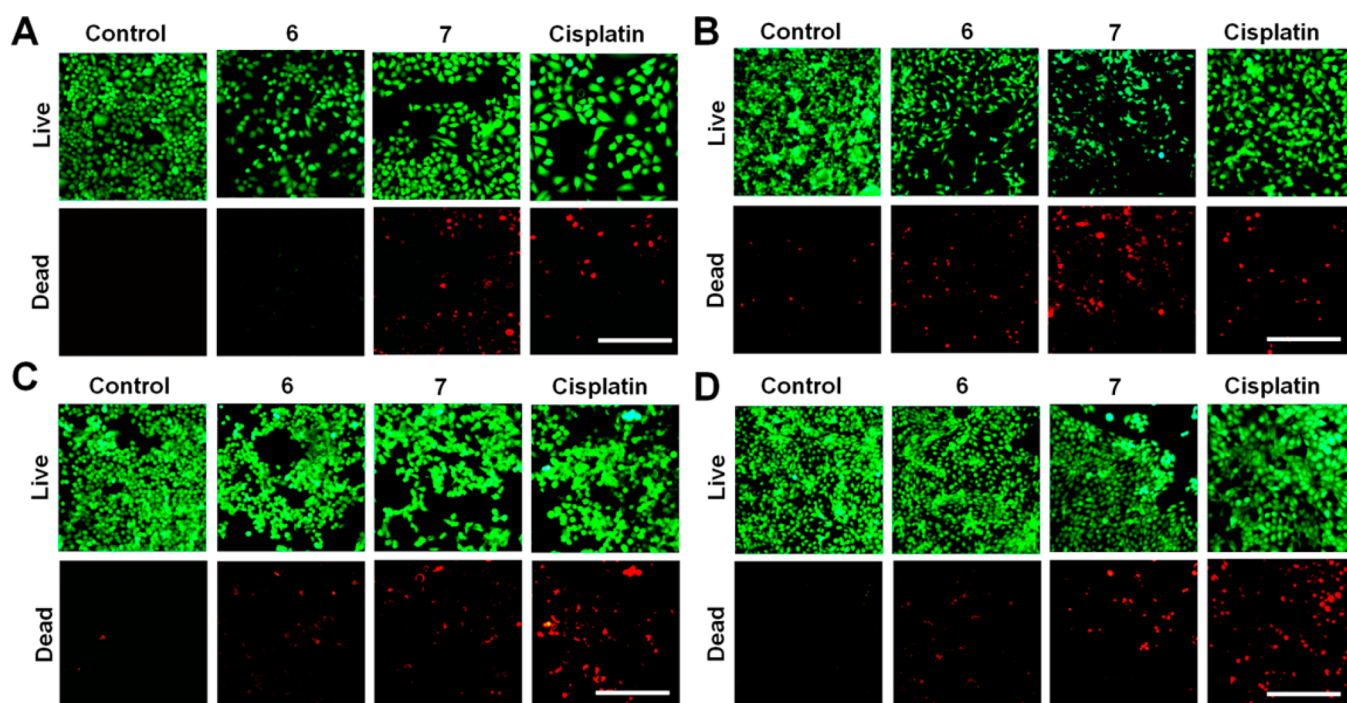


Figure 6. Live–dead cell viability assay for (A) A549, (B) MCF7, (C) KB, and (D) HaCaT cells. Cells were treated with a 10 μM concentration of each compound for 48 h and stained with live–dead fluorescent dyes. Green color staining represents live cells, whereas red color fluorescence indicates dead cells with damaged membranes. Scale bar: 200 μm .

Interestingly, **7** exhibited superior cytotoxic effects (IC_{50} values of 20.0 ± 0.2 and 05.0 ± 0.2 μM) when compared with cisplatin (IC_{50} values of 25.0 ± 0.3 and 20.0 ± 0.3 μM) for A549 and MCF7 cells, respectively (Figure 5A,B; $p < 0.01$). Moreover, **6** showed a similar effect against MCF7 cells and was more cytotoxic than cisplatin at higher concentration (30 μM ; $p < 0.05$). Overall, **6** with two additional benzene rings exhibited lower cytotoxic effects in comparison with **7**. Such variations in cytotoxic effects might be attributed to differences in the hydrophobicity and molecular weight, leading to alteration in the cellular uptake.¹⁶ Differences in the cellular uptake would allow variable access of compounds to the nuclear DNA, which might lead to inconsistent cytotoxic effects.

In order to further investigate the effect of synthesized compounds on the cell viability and attachment, cells were stained with two fluorescent dyes (Calcein AM and Ethidium homodimer-1) after 48 h with constant 10 μM concentration. Live cells were found to be firmly attached in all cases, and a variable number of dead cells were observed based on the IC_{50} concentration of each compound. A549 and KB cells were found to be swollen after treatment with **7** and cisplatin (Figure 6A,C). In contrast, no such morphological change was observed for the other two cell lines (Figure 6B,D).

Flow Cytometry Analysis. MTT data indicated that the synthesized compounds (**6** and **7** show cytotoxic effects against various human cell lines (A549, MCF7, KB, and HaCaT). We further investigated the mechanism of action of these compounds by analyzing their effects on the cell cycle and membrane integrity. Cell cycle checkpoints ensure the normal growth of cells. In the case of DNA damage, the cell cycle is arrested in that particular phase until the damaged DNA is repaired.¹⁷ Platinum (Pt)-based cytotoxic drugs are known to target the DNA replication process.¹⁸ In the present study, cisplatin treatment induced S and G2 phase arrest for all four cell types (Supporting Information S12, Figure S18). The effect

of cisplatin was in accordance with earlier reports.¹⁹ A549 cells did not show cell cycle arrest in any phase (Supporting Information S12, Figure S18A) when treated with our synthesized compounds (**6** and **7**). **7** and **6** induced cell cycle arrest in the G2 phase for MCF7 and KB cells, respectively (Supportin Information S12, Figure S18B,C), which indicates the possibility of apoptosis in these two cell lines.²⁰ A slight G1 arrest was observed for HaCaT cells after treatment with **6** and **7** (Supporting Information S12, Figure S18D). Cell cycle data indicate that cytotoxic effects of our synthesized compounds might be followed by apoptosis in certain cases where cell cycle arrest is observed.

In general, cells may follow either apoptosis or necrosis after treatment with any cytotoxic compound. Apoptosis is also known as programmed cell death and characterized by cell shrinkage, DNA fragmentation, and chromatin condensation. Necrosis, on the other hand, is induced by physical cell damage and characterized by early cell membrane damage and cellular swelling. Cells following the necrosis pathway of cell death may be identified by staining with propidium iodide (PI) dye. This dye is cell-impermeable and enters the cell only if the cell membrane is damaged. Hence, PI staining is a suitable way of assessing whether cells are undergoing necrosis.²¹ In the present study, we followed the same and all of the cells were stained with PI 48 h after treatment with each respective compound. Cells were administered to flow cytometry analysis without fixing them in ethanol. Data were acquired following a similar gating for all of the samples, and % PI-positive cells (undergoing necrosis) are reported (Supporting Information S13, Figure S19).

In all cases, cells were more sensitive to cisplatin and a higher percentage of PI-positive cells was observed after treatment compared to other groups ($p < 0.01$). However, MTT data indicated that the cytotoxic effects of **7** are comparable to those of cisplatin for A549 and MCF7 cells. This suggests that only a

fraction of macrocycle-7-treated cells are undergoing possible necrotic cell death, while the remaining population may follow the apoptotic pathway. **7** has induced membrane damage for a higher population of cells (A549 cells, $7.12 \pm 0.03\%$; KB cells, $7.31 \pm 0.41\%$) compared to **6**-treated cells (A549 cells, $5.17 \pm 0.13\%$; KB cells, $5.17 \pm 0.25\%$; Supporting Information S13, Figure S19A,C; $p < 0.01$). This might be an indication toward necrosis-induced cell death. These data are in accordance with live–dead images, where **7**-treated cells exhibited a swollen morphology (a signature of necrotic cell death; Figure 6A,C). Although MCF7 cells did not exhibit any significant difference between the two synthesized compounds (**6** and **7**), a percentage of PI-positive cells was elevated compared with the control group (Supporting Information S13, Figure S19B; $p < 0.05$). On the contrary, both compounds were ineffective against HaCaT cells, and values were comparable with those of the control group (Supporting Information S13, Figure S19D). In conclusion, data suggested that platinum-containing macrocyclic compounds (**6** and **7**) induced the loss of membrane integrity against cancer cells and might serve as a potential target for anticancer therapy.

CONCLUSION

In conclusion, we have reported two new cationic and hexagonal (irregular) macrocycles (**6** and **7**) derived from a pyrazine-based organometallic acceptor clip **5** using only four tectons in highly efficient coordination-driven self-assembly reactions. **6** and **7** were characterized by well-known spectroscopic techniques, and one of the macrocycles (**6**) was characterized by single-crystal XRD analysis. The macrocycles were tested against A549 (human lung carcinoma cell line), KB (human oral cancer cell line), MCF7 (human breast cancer cell line), and HaCaT (human skin keratinocyte cell line) and compared with cisplatin. It was observed that the smaller macrocycle (**7**) has superior cytotoxic effects against all cancer cells and its IC_{50} concentration is lower relative to cisplatin for A549 and MCF7 cells. This report is a unique example, wherein self-assembled two-dimensional ensembles derived from a platinum(II) acceptor clip have been studied for their potential application in anticancer therapy.

EXPERIMENTAL SECTION

General Details. All chemicals and anhydrous solvents used in this work were purchased from commercial sources and used without further purification. Triethylamine was freshly distilled prior to use. **1** was prepared by following the reported literature procedures.²² A549 (human lung carcinoma cell line), KB (human oral cancer cell line), MCF7 (human breast cancer cell line), and HaCaT (human skin keratinocyte cell line) were purchased from National Centre for Cell Science, Pune, India. All of the cells were cultured and maintained in Dulbecco's modified Eagle medium (Gibco, USA) containing a 1% (v/v) antibiotic–antimycotic solution (Himedia, India) and 10% (v/v) fetal bovine serum (FBS; Gibco, USA) in a humidified CO₂ incubator at 37 °C. Phosphate-buffered saline (PBS) and Ribonuclease A (RNaseA) were purchased from Sigma-Aldrich, USA. FT-IR spectra were recorded in a PerkinElmer Spectrum 400 FT-IR spectrophotometer. ¹H and ³¹P NMR spectra were recorded on Bruker 400/500 MHz spectrometers. Elemental analyses were carried out using an Elementar Vario Micro Cube elemental analyzer. ESI-MS analysis was performed using a Bruker Impact ESI-Q-TOF system. A Tecan infinite Pro M 200 reader with *i-control* software was used for to record the absorbance. A EVOS FL (Life Technologies, USA) fluorescence microscope was used.

Synthesis of Compound 2. A solution of compounds 1,3-diiodobenzene (1.03 g, 3.12 mmol) and palladium tetrakis-

(triphenylphosphine) (91 mg, 0.08 mmol) in triethylamine (25 mL) was stirred at room temperature for 20 min in a nitrogen atmosphere. Then cuprous(I) iodide (30 mg, 0.16 mmol) was added, followed by alkyne **1** (0.2 g, 0.78 mmol). The solution was heated overnight at 55 °C. Subsequently, the reaction mixture was quenched with ammonium chloride, extracted with dichloromethane, and washed with brine. The organic phase was dried by sodium sulfate and concentrated with a rotary evaporator. The crude product was purified by column chromatography over 100–200 mesh silica gel using 6% ethyl acetate in hexane to obtain the product as a white solid. Yield: 0.35 g, 84%. Mp: 173–175 °C. ¹H NMR (CDCl₃, 400 MHz): δ 8.65 (s, 2H, Ar–H), 7.99–7.98 (m, 2H, Ar–H), 7.77–7.74 (m, 2H, Ar–H), 7.59–7.57 (m, 2H, Ar–H), 7.15–7.11 (m, 2H, Ar–H). ¹³C NMR (CDCl₃, 100 MHz): δ 145.7, 140.7, 139.4, 138.7, 131.3, 130.0, 123.3, 93.7, 91.7, 86.4. IR (ATR): 2218, 1544, 1506, 1465, 1408, 1166, 1141, 1060, 877, 776, 673 cm⁻¹. Anal. Calcd for C₂₀H₁₀I₂N₂: C, 51.96; H, 4.40; N, 3.97. Found: C, 51.88; H, 4.35; N, 3.92. MS (ESI). Calcd (21.7%; M⁺): m/z 532.12. Found: m/z 532.90.

Synthesis of Compound 4. In a 100 mL round-bottomed Schlenk flask, **2** (0.5 g, 0.94 mmol), tetrakis(triphenylphosphine)palladium (0.22 g, 0.19 mmol), and 46 mg of cuprous(I) iodide (54 mg, 0.28 mmol) were added in 30 mL of dry THF. Then 5 mL of dry triethylamine and (trimethylsilyl)acetylene (0.5 mL, 3.76 mmol) were added to the reaction mixture. The suspension was stirred for 16 h at room temperature in the absence of light. After removal of the solvent, the residue was washed twice with water and the organic phase was dried over sodium sulfate. The solvent was removed in a rotary evaporator, and the residue was purified by column chromatography on 100–200 mesh silica gel. The desired product **3** (0.34 g, 76%) was isolated with 3% ethyl acetate in hexane.

Desilylation of **3** (0.34 g, 0.72 mmol) was carried out in a THF solution (10 mL) using TBAF (0.46 g, 1.44 mmol) as a deprotecting agent for 5 min. The solution was evaporated in a rotary evaporator followed by washing of the residual product with water and extraction with dichloromethane. The organic phase was dried by sodium sulfate, and the solvent was removed. Finally, the desired product **4** was obtained as a white solid by purification using column chromatography on 100–200 mesh silica gel using 5% ethyl acetate in hexane.

Yield: 0.20 g, 84%. Mp: 145–147 °C. ¹H NMR (CDCl₃, 400 MHz): δ 8.66 (s, 2H, Ar–H), 7.75–7.74 (m, 2H), 7.61–7.58 (m, 2H, Ar–H), 7.54–7.52 (s, 2H, Ar–H), 7.38–7.34 (m, 2H, Ar–H). ¹³C NMR (CDCl₃, 75 MHz): δ 145.7, 139.5, 135.6, 133.2, 132.3, 128.6, 122.8, 121.7, 92.4, 85.9, 82.3, 78.3. IR (ATR): 3290, 3209, 2212, 1504, 1473, 1207, 1163, 1004, 894, 783, 677 cm⁻¹. Anal. Calcd for C₂₄H₁₂N₂: C, 87.79; H, 3.68; N, 8.53. Found: C, 87.86; H, 3.76; N, 8.63. MS (ESI). Calcd (26.7%; M⁺): m/z 328.37. Found: m/z 329.10.

Synthesis of Compound 5. **4** (0.1 g, 0.30 mmol) and *trans*-diiodobis(triethylphosphine)platinum(II) (0.63 g, 0.91 mmol) were placed in a 100 mL Schlenk flask in the glovebox. Subsequently, 30 mL of dry toluene and 10 mL of freshly distilled triethylamine were added under nitrogen. The solution was stirred for 20 min at room temperature before CuI (9 mg, 0.05 mmol) was added in one portion. The reaction mixture was stirred overnight at room temperature. Triethylammonium iodide precipitated from the solution and was removed by filtration. Toluene was evaporated in a rotary evaporator, and the resulting yellow residue was purified by column chromatography on 100–200 mesh silica gel by eluting with 3% ethyl acetate in hexane first and then gradually increasing the polarity of the eluant to 8% ethyl acetate in hexane to isolate **5** as a yellow semisolid.

Yield: 0.3 g, 68%. ¹H NMR (400 MHz, CDCl₃): δ 8.64 (s, 2H, Ar–H), 7.50 (s, 2H, Ar–H), 7.42–7.40 (d, $J = 7.6$ Hz, 2H, Ar–H), 7.31 (s, 2H, Ar–H), 7.24 (s, 2H, Ar–H), 2.26–2.19 (m, 24H, –CH₂), 1.22–1.14 (m, 36H, –CH₃). ¹³C NMR (CDCl₃, 75 MHz): δ 145.4, 139.5, 133.9, 131.6, 129.0, 128.3, 121.1, 99.1, 93.5, 91.9, 85.2, 16.6, 8.1. ³¹P{¹H} NMR (163 MHz, CDCl₃): δ 8.59 ($J_{\text{P-Pt}} = 1165$ Hz). IR (ATR): 2957, 2927, 2872, 2210, 2113, 1587, 1506, 1454, 1408, 1217, 1145, 1031, 1004, 887, 767, 727, 680 cm⁻¹. MS (ESI). Calcd (M⁺ + 1): m/z 1442.19. Found: m/z 1443.5.

General Procedure for the Synthesis of Macrocycles 6 and 7. To the solution of compound **5** (100 mg, 0.07 mmol) in chloroform

(4 mL) was added AgNO₃ (24 mg, 0.14 mmol) in one portion, and the reaction mixture was stirred overnight in the absence of light at room temperature. The precipitated AgI was filtered over a bed of Celite, and the filtrate was collected as a yellow solution. Subsequently, a methanolic solution of the respective donor tecton (bipyridine and pyrazine; 0.02 mmol, 0.5 mL) was added dropwise to the aforementioned filtrate with continuous stirring. The reaction mixture was stirred for 15 h at room temperature. Solvents were removed on a rotary evaporator, and the product obtained was washed several times with *n*-pentane to obtain a yellow solid, which was finally dried in a vacuum. **6** was crystallized by slow vapor diffusion of diethyl ether in its corresponding concentrated dichloromethane-methanol solution and **7** was crystallized as a yellow microcrystalline solid by vapor diffusion of diethyl ether in its corresponding concentrated methanol solution.

Macrocycle 6. Yield: 30 mg, 92%. ¹H NMR (400 MHz, CDCl₃): δ 8.89–8.88 (d, *J* = 6.52 Hz, 8H, Ar–H), 8.67 (s, 4H, Ar–H), 8.66–8.64 (d, *J* = 6.72 Hz, 8H, Ar–H), 7.64 (s, 4H, Ar–H), 7.45–7.44 (m, 4H, Ar–H), 7.32–7.31 (m, 8H, Ar–H), 1.85–1.81 (m, 48H, –CH₂–), 1.26–1.17 (m, 72H, –CH₃). ¹³C NMR (CDCl₃, 75 MHz): δ 153.3, 152.6, 150.4, 145.8, 144.8, 139.5, 135.5, 131.6, 128.3, 126.3, 121.1, 93.1, 85.9, 14.3, 7.7. ³¹P{¹H} NMR (162 MHz, CDCl₃): δ 15.88 (¹*J*_{PPt} = 1164 Hz). IR (ATR): 2970, 2931, 2870, 2214, 2121, 1705, 1635, 1581, 1504, 1458, 1327, 1157, 1033, 887, 756, 740 cm⁻¹. Anal. Calcd for C₁₁₆H₁₅₆N₈P₈Pt₄: C, 51.78; H, 5.84; N, 4.16. Found: C, 51.89; H, 5.98; N, 4.23. MS (ESI). Calcd for [M – 2NO₃]²⁺: *m/z* 1406.32. Found: *m/z* 1406.43. Calcd for [M – 3NO₃]³⁺: *m/z* 916.88. Found: *m/z* 916.59. Calcd for [M – 4NO₃]⁴⁺: *m/z* 672.16. Found: *m/z* 672.22.

Macrocycle 7. Yield: 28 mg, 91%. ¹H NMR (400 MHz, CDCl₃): δ 8.65 (s, 4H, Ar–H), 8.60 (s, 8H, Ar–H), 7.44 (s, 4H, Ar–H), 7.40–7.38 (m, 8H, Ar–H), 7.25–7.24 (m, 4H, Ar–H), 1.99–1.93 (m, 48H, –CH₂–), 1.27–1.25 (m, 72H, –CH₃). ¹³C NMR (CDCl₃, 75 MHz): δ 145.7, 145.4, 144.8, 134.9, 134.5, 132.3, 129.3, 128.7, 121.1, 93.5, 85.2, 14.3, 7.7. ³¹P{¹H} NMR (162 MHz, CDCl₃): δ 20.13 (¹*J*_{PPt} = 1238 Hz). IR (ATR): 2972, 2924, 2875, 2223, 2124, 1640, 1583, 1463, 1331, 1273, 1149, 1038, 885, 752, 738 cm⁻¹. Anal. Calcd for C₁₀₄H₁₄₈N₈P₈Pt₄: C, 50.53; H, 5.86; N, 4.29. Found: C, 50.70; H, 5.94; N, 5.92. MS (ESI). Calcd for [M – 2NO₃]²⁺: *m/z* 1330.40. Found: 1330.42. Calcd for [M – 3NO₃]³⁺: *m/z* 866.27. Found: *m/z* 866.28. Calcd for [M – 4NO₃]⁴⁺: *m/z* 634.20. Found: *m/z* 634.21.

Crystallographic Data Collection and Refinement. Single-crystal data for **4** and **6** were collected on a Bruker D8 Quest diffractometer equipped with a PHOTON 100 CMOS detector, using a graphite monochromator and Mo K α (λ = 0.71073 Å) radiation operating at 50 kV and 30 mA. The unit cell measurement, data collection (φ and ω scan), integration, scaling and absorption corrections for the crystals were done using Bruker *Apex II* software.²³ The structures were solved using a direct method, followed by full matrix least-squares refinements against *F*² (all data in HKLF 4 format) using *SHELXTL*.²⁴ A multiscan absorption correction, based on equivalent reflections, was applied to the data. All of the atoms except platinum and phosphorus atoms were refined isotropically. There are two disordered nitrate anions, which were isotropically refined. The contributions of the most disordered solvent molecules and counteranions (NO₃⁻) were removed from the diffraction data using the *SQUEEZE* routine of *PLATON* software,²⁵ and then final refinements were carried out.

Crystallographic data for “data collection and structure refinement parameters” and crystallographic data for **4** and **6** are summarized in [Supporting Information S8](#).

CCDC contains the supplementary crystallographic data for this paper with deposition numbers of CCDC 1518730 and 1518833 for compounds **4** and **6**, respectively.

Preparation of Stock Solutions. 1 mM stock solutions of both compounds (**6** and **7**) were prepared in DMSO (Sigma-Aldrich, USA), whereas a cisplatin stock solution was prepared in normal saline (0.9% sodium chloride). For cell culture experiments, 0.1–3% (v/v) of a stock solution was used.

In Vitro Cytotoxicity. The cytotoxic activities of both compounds **6** and **7** was tested against A549, MCF7, KB, and HaCaT cell lines at varying concentrations ranging from 1 to 30 μ M. Cells were seeded in a 96-well flat-bottom plate, keeping a similar cell density ($\sim 10^4$) in each well, and allowed to adhere for 24 h. Cells were further treated with predefined concentrations of compounds **6** and **7** and cisplatin. After 48 h of treatment, the viability of the cells was quantified by measuring their metabolic activity using MTT assay [3-(4,5-dimethylthiazol-2-yl)-2,5-diphenyltetrazolium bromide]. A 10% (v/v) MTT stock solution (5 mg/mL) prepared in FBS free culture media was added to the compound-treated cells and incubated for 4 h to allow formazan crystal formation. These crystals were further dissolved in 200 μ L of DMSO, and the absorbance was measured at 570 nm using a microplate reader. The absorbance values of compound-treated cells were normalized with the untreated control group, and a five-point dose-dependent curve was plotted to calculate the IC₅₀ value of each compound (the IC₅₀ value is the concentration of the compound at which 50% of cells are viable).

The viability of cells after 48 h of compound treatment (10 μ M concentration) was assessed by staining the cells with a live–dead solution. Cells were incubated with a working live–dead solution (1 μ L of 4 mM Calcein AM and 4 μ L of 2 mM Ethidium homodimer-1 in 2 mL of PBS) for 10 min at 37 °C in a humidified CO₂ incubator. Calcein AM enters into live cells, which, in turn, undergoes ester hydrolysis by a cellular esterase enzyme and fluoresces green (excitation = 495 nm; emission = 516 nm). On the other hand, Ethidium homodimer-1 specifically enters into dead cells, and, upon binding with DNA, gives red fluorescence (excitation = 528 nm; emission = 617 nm). Stained cells were washed three times with sterile PBS and imaged under a fluorescent microscope.

Flow Cytometry. Cell Cycle Analysis. Cells treated with compound were tested for any cell cycle arrest using flow cytometry. Approximately 2×10^5 cells were seeded in each well of standard 6-well tissue culture plates, and cells were allowed to adhere for 24 h in a humidified incubator. Further, cells were treated with IC₅₀ concentration of each compound for 48 h. After compound exposure, cells were harvested and a cell pellet was fixed in ice cold 70% ethanol and stored at –20 °C for further analysis. Fixed cells were washed twice with PBS and incubated with RNaseA [200 μ g/mL (w/v)] for 1 h at room temperature. RNaseA treatment helps to avoid nonspecific interaction of PI with nucleic acids. After RNaseA treatment, 40 μ g/mL PI was added to the samples, and they were incubated on ice for 10 min. Cytometry acquisition was done on a BD Accuri C6 plus flow cytometer with a blue laser (488 nm) on the FL2 channel. Data were analyzed using a ModFit LT, version 2.0 (Verity Software House), to calculate the percentage of cells present in each phase of the cell cycle.

Live PI Staining. In order to analyze the membrane integrity of compound-treated cells, cells were stained with PI dye. PI is a cell-impermeable dye and stains only dead cells of a damaged cellular membrane. Cells were cultured and treated with a specific concentration of each compound as described earlier. After treatment, cells were harvested and centrifuged at 1000 rpm for 5 min. A cell pellet was washed three times with sterile PBS and resuspended in the same. Each cell pellet was further treated with PI [15 μ g/mL (w/v) final concentration] at 4 °C for 10 min and vortexed gently. Cytometry data acquisition was performed using a BD Accuri C6 plus flow cytometer with a blue laser (488 nm) on the FL2 channel.

Statistical Analysis. All of the biological experiments (including MTT assay and flow cytometry analysis) were performed in triplicate. Significant differences among different experimental groups at various time points were assessed by performing one-way analysis of variance (ANOVA) following Tukey’s test using *Origin 8.0* software. The significance level was analyzed at both 95% and 99% confidence levels. *p* < 0.05 was considered to be significant and *p* < 0.01 highly significant.

■ ASSOCIATED CONTENT

● Supporting Information

The Supporting Information is available free of charge on the ACS Publications website at DOI: 10.1021/acs.inorgchem.7b01561.

¹H and ¹³C{¹H} NMR spectra of compounds 2 and 4, ¹H and ³¹P{¹H} NMR spectra of compounds 5–7, ESI-MS analysis of macrocycles 6 and 7, X-ray crystallography analysis of compound 4 and macrocycle 6 (PDF)

■ Accession Codes

CCDC 1518730 and 1518833 contain the supplementary crystallographic data for this paper. These data can be obtained free of charge via www.ccdc.cam.ac.uk/data_request/cif, or by emailing data_request@ccdc.cam.ac.uk, or by contacting The Cambridge Crystallographic Data Centre, 12 Union Road, Cambridge CB2 1EZ, UK; fax: +44 1223 336033.

■ AUTHOR INFORMATION

■ Corresponding Authors

*E-mail: biman.mandal@iitg.ernet.in or mandal.biman@gmail.com (B.B.M.). Tel.: +91-361-258 2225.

*E-mail: neeladri@iitp.ac.in or neeladri2002@yahoo.co.in (N.D.). Tel.: +91-9631624708.

■ ORCID

Biman B. Mandal: 0000-0003-3936-4621

Neeladri Das: 0000-0003-3476-1097

■ Notes

The authors declare no competing financial interest.

■ ACKNOWLEDGMENTS

N.D. thanks the Indian Institute of Technology (IIT) Patna for financial support. S.B. thanks IIT Patna for an Institute Research Fellowship. A.J. and K.S. thank UGC, New Delhi, India, for a Research Fellowship. The authors also acknowledge SAIF-Panjab University and SAIF-IIT Patna for analytical facilities. B.B.M. gratefully acknowledges funding support through the Department of Biotechnology and Department of Science and Technology, Government of India.

■ REFERENCES

(1) (a) Cook, T. R.; Stang, P. J. Recent Developments in the Preparation and Chemistry of Metallacycles and Metallacages via Coordination. *Chem. Rev.* **2015**, *115*, 7001. (b) Cook, T. R.; Zheng, Y.-R.; Stang, P. J. Metal–Organic Frameworks and Self-Assembled Supramolecular Coordination Complexes: Comparing and Contrasting the Design, Synthesis, and Functionality of Metal–Organic Materials. *Chem. Rev.* **2013**, *113*, 734. (c) Schoedel, A.; Zaworotko, M. J. [M₃(μ₃-O)(O₂CR)₆] and related trigonal prisms: versatile molecular building blocks for crystal engineering of metal–organic material platforms. *Chem. Sci.* **2014**, *5*, 1269. (d) Tanaka, S.; Tsurugi, H.; Mashima, K. Supramolecular assemblies of multi-nuclear transition metal complexes: Synthesis and redox properties. *Coord. Chem. Rev.* **2014**, *265*, 38. (e) Schmidt, A.; Casini, A.; Kuhn, F. E. Self-assembled M₂L₄ coordination cages: Synthesis and potential applications. *Coord. Chem. Rev.* **2014**, *275*, 19. (f) Chakraborty, R.; Mukherjee, P. S.; Stang, P. J. Supramolecular Coordination: Self-Assembly of Finite Two- and Three-Dimensional Ensembles. *Chem. Rev.* **2011**, *111*, 6810. (g) Li, S.; Huang, J.; Cook, T. R.; Pollock, J. B.; Kim, H.; Chi, K.-W.; Stang, P. J. Formation of [3]Catenanes from 10 Precursors via Multicomponent Coordination-Driven Self-Assembly of Metallarectangles. *J. Am. Chem. Soc.* **2013**, *135*, 2084. (h) Wang, W.; Wang, Y.-X.; Yang, H.-B. Supramolecular transformations within discrete coordination-driven supramolecular architectures. *Chem. Soc. Rev.* **2016**, *45*, 2656.

(i) Fiedler, D.; Leung, D. H.; Bergman, R. G.; Raymond, K. N. Selective Molecular Recognition, C–H Bond Activation, and Catalysis in Nanoscale Reaction Vessels. *Acc. Chem. Res.* **2005**, *38*, 349. (j) Spokoiny, A. M.; Kim, D.; Sumrein, A.; Mirkin, C. A. Infinite coordination polymer nano- and microparticle structures. *Chem. Soc. Rev.* **2009**, *38*, 1218. (k) Bhowmick, S.; Chakraborty, S.; Das, A.; Rajamohanam, P. R.; Das, N. Pyrazine-Based Organometallic Complex: Synthesis, Characterization, and Supramolecular Chemistry. *Inorg. Chem.* **2015**, *54*, 2543. (l) Bhowmick, S.; Chakraborty, S.; Das, A.; Nallapeta, S.; Das, N. Pyrazine Motif Containing Hexagonal Macrocyces: Synthesis, Characterization, and Host–Guest Chemistry with Nitro Aromatics. *Inorg. Chem.* **2015**, *54*, 8994. (m) Jana, A.; Bhowmick, S.; Kaur, S.; Kashyap, H. K.; Das, N. Design of a flexible organometallic tecton: host–guest chemistry with picric acid and self-assembly of platinum macrocycles. *Dalton Trans.* **2017**, *46*, 1986.

(2) (a) Chen, L.-J.; Jiang, B.; Yang, H.-B. Transformable nanostructures of cholesteryl-containing rhomboidal metallacycles through hierarchical self-assembl. *Org. Chem. Front.* **2016**, *3*, 579. (b) Lehn, J. M. Toward complex matter: Supramolecular chemistry and self-organization. *Proc. Natl. Acad. Sci. U. S. A.* **2002**, *99*, 4763. (c) Leigh, D. A.; Pritchard, R. G.; Stephens, A. J. A Star of David catenane. *Nat. Chem.* **2014**, *6*, 978. (d) Jana, A.; Das, N. Self-Assembly of [2 + 2] Platina Macrocycles Using a Flexible Organometallic Clip. *Chemistryselect* **2017**, *2*, 4099. (e) Tian, J.; Zhou, T.-Y.; Zhang, S.-C.; Aloni, S.; Altoe, M. V.; Xie, S.-H.; Wang, H.; Zhang, D.-W.; Zhao, X.; Liu, Y.; Li, Z.-T. Three-dimensional periodic supramolecular organic framework ion sponge in water and microcrystals. *Nat. Commun.* **2014**, *5*, 5574. (f) Li, S.-H.; Zhang, H.-Y.; Xu, X.; Liu, Y. Mechanically selflocked chiral gemini-catenanes. *Nat. Commun.* **2015**, *6*, 7590. (g) Bhowmick, S.; Chakraborty, S.; Marri, S. R.; Behera, J. N.; Das, N. Pyrazine-based donor tectons: synthesis, self-assembly and characterization. *RSC Adv.* **2016**, *6*, 8992. (h) Chakraborty, S.; Mondal, S.; Bhowmick, S.; Ma, J.; Tan, H.; Neogi, S.; Das, N. Triptycene based organometallic complexes: a new class of acceptor synthons for supramolecular ensembles. *Dalton Trans.* **2014**, *43*, 13270.

(3) (a) Lehn, J.-M. *Supramolecular Chemistry: Concepts and Perspectives*; Wiley-VCH: Weinheim, Germany, 1995. (b) Han, M.; Engelhard, D. M.; Clever, G. H. Self-assembled coordination cages based on banana-shaped ligands. *Chem. Soc. Rev.* **2014**, *43*, 1848. (c) Ward, M. D.; Raithby, P. R. Functional behaviour from controlled self-assembly: challenges and prospects. *Chem. Soc. Rev.* **2013**, *42*, 1619. (d) Liu, S.; Han, Y.-F.; Jin, G.-X. Formation of direct metal–metal bonds from 16-electron “pseudo-aromatic” half-sandwich complexes Cp[∞]M[E₂C₂(B₁₀H₁₀)]. *Chem. Soc. Rev.* **2007**, *36*, 1543. (e) Galstyan, A.; Sanz Miguel, P. J.; Weise, K.; Lippert, B. Discrete and polymeric heteronuclear constructs derived from triangular 2,2′-bipyrazine complexes of cis-a₂Pt^{II} (with a = NH₃ or a₂ = en). *Dalton Trans.* **2013**, *42*, 16151. (f) Alberti, F. M.; Zielinski, W.; Morell Cerda, M.; Sanz Miguel, P. J.; Troeppner, O.; Ivanovic-Burmazovic, I.; Lippert, B. Stepwise Coordination of Pt^{II}-180° and Pd^{II}-90° Metal Fragments to the Purine Nucleobase 9-Methylhypoxanthine Affords a Closed Octadecanuclear Pt₆Pd₁₂ Cluster. *Chem. - Eur. J.* **2013**, *19*, 9800. (g) Li, Y.; Jiang, Z.; Yuan, J.; Liu, D.; Wu, T.; Moorefield, C. N.; Newkome, G. R.; Wang, P. Facile thermodynamic conversion of a linear metallopolymer into a self-assembled hexameric metallomacrocycle. *Chem. Commun.* **2015**, *51*, 5766. (h) Sarkar, R.; Guo, K.; Moorefield, C. N.; Saunders, M. J.; Wesdemiotis, C.; Newkome, G. R. One-step multicomponent self-assembly of a first-generation Sierpiński triangle: from fractal design to chemical reality. *Angew. Chem., Int. Ed.* **2014**, *53*, 12182. (i) Saha, M. L.; Neogi, S.; Schmittel, M. Dynamic heteroleptic metal-phenanthroline complexes: from structure to function. *Dalton Trans.* **2014**, *43*, 3815. (j) Chen, L.; Chen, Q.; Wu, M.; Jiang, F.; Hong, M. Controllable Coordination-Driven Self-Assembly: From Discrete Metallocages to Infinite Cage-Based Frameworks. *Acc. Chem. Res.* **2015**, *48*, 201. (k) Chakraborty, S.; Mondal, S.; Li, Q.; Das, N. Synthesis and characterization of triptycene based tripods and design of a metallasupramolecular cage. *Tetrahedron Lett.* **2013**, *54*, 1681. (l) Ludlow, J. M., III; Tominaga, M.; Chujo, Y.; Schultz, A.; Lu, X.; Xie, T.; Guo, K.; Moorefield, C. N.; Wesdemiotis,

C.; Newkome, G. R. Self-assembly of a family of suprametallomacrocycles: revisiting an o-carborane bisterpyridyl building block. *Dalton Trans.* **2014**, 43, 9604. (m) Chakraborty, S.; Bhowmick, S.; Ma, J.; Tan, H.; Das, N. Size dependent effect of new organometallic triptycene tectons on the dimensions of self-assembled macrocycles. *Inorg. Chem. Front.* **2015**, 2, 290.

(4) (a) Yoshizawa, M.; Klosterman, J. K. Molecular architectures of multi-anthracene assemblies. *Chem. Soc. Rev.* **2014**, 43, 1885. (b) Oliveri, C. G.; Ulmann, P. A.; Wiester, M. J.; Mirkin, C. A. Heteroligated Supramolecular Coordination Complexes Formed via the Halide-Induced Ligand Rearrangement Reaction. *Acc. Chem. Res.* **2008**, 41, 1618. (c) Newkome, G. R.; Shreiner, C. Dendrimers Derived from 1 → 3 Branching Motifs. *Chem. Rev.* **2010**, 110, 6338. (d) Stang, P. J.; Olenyuk, B. Self-Assembly, Symmetry, and Molecular Architecture: Coordination as the Motif in the Rational Design of Supramolecular Metallacyclic Polygons and Polyhedra. *Acc. Chem. Res.* **1997**, 30, 502. (e) Leininger, S.; Olenyuk, B.; Stang, P. J. Self-Assembly of Discrete Cyclic Nanostructures Mediated by Transition Metals. *Chem. Rev.* **2000**, 100, 853. (f) Wang, W.; Sun, B.; Wang, X.-Q.; Ren, Y.-Y.; Chen, L.-J.; Ma, J.; Zhang, Y.; Li, X.; Yu, Y.; Tan, H.; Yang, H.-B. Discrete Stimuli-Responsive Multirotaxanes with Supramolecular Cores Constructed through a Modular Approach. *Chem. - Eur. J.* **2015**, 21, 6286. (g) Fujita, M.; Tominaga, M.; Hori, A.; Therrien, B. Coordination Assemblies from a Pd(II)-Cornered Square Complex. *Acc. Chem. Res.* **2005**, 38, 369. (h) Inokuma, Y.; Kawano, M.; Fujita, M. Crystalline molecular flasks. *Nat. Chem.* **2011**, 3, 349. (i) Yoshizawa, M.; Klosterman, J. K.; Fujita, M. Functional Molecular Flasks: New Properties and Reactions within Discrete, Self-Assembled Hosts. *Angew. Chem., Int. Ed.* **2009**, 48, 3418. (j) Harris, K.; Fujita, D.; Fujita, M. Giant hollow MnL₂n spherical complexes: structure, functionalisation and applications. *Chem. Commun.* **2013**, 49, 6703. (k) Xu, X.-D.; Yao, C.-J.; Chen, L.-J.; Yin, G.-Q.; Zhong, Y.-W.; Yang, H.-B. Facile Construction of Structurally Defined Porous Membranes from Supramolecular Hexakistriphenylamine Metallacycles through Electropolymerization. *Chem. - Eur. J.* **2016**, 22, S211.

(5) (a) Rosenberg, B.; VanCamp, L.; Trosko, J. E.; Mansour, V. H. Platinum Compounds: a New Class of Potent Antitumour Agents. *Nature* **1969**, 222, 385. (b) Canetta, R.; Rozenzweig, M.; Carter, S. K. Carboplatin: the clinical spectrum to date. *Cancer Treat. Rev.* **1985**, 12, 125. (c) Vickers, A. E. M.; Rose, K.; Fisher, R.; Saulnier, M.; Sahota, P.; Bentley, P. Kidney slices of human and rat to characterize cisplatin-induced injury on cellular pathways and morphology. *Toxicol. Pathol.* **2004**, 32, 577. (d) Misset, J. L.; Bleiberg, H.; Sutherland, W.; Bekradda, M.; Cvitkovic, E. Oxaliplatin clinical activity: a review. *Crit. Rev. Oncol. Hematol.* **2000**, 35, 75.

(6) (a) Kelland, L. The resurgence of platinum-based cancer chemotherapy. *Nat. Rev. Cancer* **2007**, 7, 573. (b) Jung, Y.; Lippard, S. J. Direct Cellular Responses to Platinum-Induced DNA Damage. *Chem. Rev.* **2007**, 107, 1387. (c) Todd, R. C.; Lippard, S. J. Inhibition of transcription by platinum antitumor compounds. *Metallics* **2009**, 1, 280. (d) Yao, X.; Panichpisal, K.; Kurtzman, N.; Nugent, K. Cisplatin nephrotoxicity: a review. *Am. J. Med. Sci.* **2007**, 334, 115. (e) McWhinney, S. R.; Goldberg, R. M.; McLeod, H. L. Platinum neurotoxicity pharmacogenetics. *Mol. Cancer Ther.* **2009**, 8, 10. (f) Abu-Surrah, A. S.; Kettunen, M. Platinum group antitumor chemistry: design and development of new anticancer drugs complementary to cisplatin. *Curr. Med. Chem.* **2006**, 13, 1337. (g) Wang, X. Y.; Guo, Z. J. Towards the rational design of platinum(II) and gold(III) complexes as antitumour agents. *Dalton Trans.* **2008**, 1521. (h) Rabik, A.; Dolan, M. E. Molecular mechanisms of resistance and toxicity associated with platinating agents. *Cancer Treat. Rev.* **2007**, 33, 9.

(7) (a) Wong, E.; Giandomenico, C. M. Current Status of Platinum-Based Antitumor Drugs. *Chem. Rev.* **1999**, 99, 2451. (b) Wheate, N. J.; Walker, S.; Craig, G. E.; Oun, R. The status of platinum anticancer drugs in the clinic and in clinical trials. *Dalton Trans.* **2010**, 39, 8113. (c) Mangrum, J. B.; Farrell, N. P. Excursions in polynuclear platinum DNA binding. *Chem. Commun.* **2010**, 46, 6640. (d) Mishra, A.; Chang Lee, S.; Kaushik, N.; Cook, T. R.; Choi, E. H.; Kumar Kaushik, N.;

Stang, P. J.; Chi, K.-W. Self-Assembled Supramolecular Hetero-Bimetallics for Anticancer Potency by Intracellular Release. *Chem. - Eur. J.* **2014**, 20, 14410. (e) Grishagin, I. V.; Pollock, J. B.; Kushal, S.; Cook, T. R.; Stang, P. J.; Olenyuk, B. Z. In vivo anticancer activity of rhomboidal Pt(II) metallacycles. *Proc. Natl. Acad. Sci. U. S. A.* **2014**, 111, 18448. (f) Vajpayee, V.; Lee, S. M.; Park, J. W.; Dubey, A.; Kim, H.; Cook, T. R.; Stang, P. J.; Chi, K.-W. Growth Inhibitory Activity of a Bis-Benzimidazole-Bridged Arene Ruthenium Metalla-Rectangle and – Prism. *Organometallics* **2013**, 32, 1563. (g) Dubey, A.; Min, J. W.; Koo, H. J.; Kim, H.; Cook, T. R.; Kang, S. C.; Stang, P. J.; Chi, K.-W. Anticancer Potency and Multidrug-Resistant Studies of Self-Assembled Arene–Ruthenium Metallarectangles. *Chem. - Eur. J.* **2013**, 19, 11622.

(8) (a) Linares, F.; Galindo, M. A.; Galli, S.; Romero, M. A.; Navarro, J. A. R.; Barea, E. Tetranuclear Coordination Assemblies Based on Half-Sandwich Ruthenium(II) Complexes: Noncovalent Binding to DNA and Cytotoxicity. *Inorg. Chem.* **2009**, 48, 7413. (b) Galanski, M.; Jakupec, M.; Keppler, B. Update of the preclinical situation of anticancer platinum complexes: novel design strategies and innovative analytical approaches. *Curr. Med. Chem.* **2005**, 12, 2075.

(9) Cook, T. R.; Vajpayee, V.; Lee, M. H.; Stang, P. J.; Chi, K.-W. Biomedical and Biochemical Applications of Self-Assembled Metallacycles and Metallacages. *Acc. Chem. Res.* **2013**, 46, 2464.

(10) (a) Vajpayee, V.; Lee, S.; Kim, S.-H.; Kang, S. C.; Cook, T. R.; Kim, H.; Kim, D. W.; Verma, S.; Lah, M. S.; Kim, I. S.; Wang, M.; Stang, P. J.; Chi, K.-W. Self-assembled metalla-rectangles bearing azodipyridyl ligands: synthesis, characterization and antitumor activity. *Dalton Trans.* **2013**, 42, 466. (b) Mattsson, J.; Govindaswamy, P.; Renfrew, A. K.; Dyson, P. J.; Štěpnička, P.; Süss-Fink, G.; Therrien, B. Synthesis, Molecular Structure, and Anticancer Activity of Cationic Arene Ruthenium Metallarectangles. *Organometallics* **2009**, 28, 4350. (c) Vajpayee, V.; Yang, Y. J.; Kang, S. C.; Kim, H.; Kim, I. S.; Wang, M.; Stang, P. J.; Chi, K.-W. Hexanuclear self-assembled arene-ruthenium nano-prismatic cages: potential anticancer agents. *Chem. Commun.* **2011**, 47, 5184. (d) Ajibola Adeyemo, A.; Shettar, A.; Bhat, I. A.; Kondaiah, P.; Mukherjee, P. S. Self-Assembly of Discrete Ru^{II}₈ Molecular Cages and Their in Vitro Anticancer Activity. *Inorg. Chem.* **2017**, 56, 608. (e) Singh, N.; Jang, S.; Jo, J.-H.; Kim, D. H.; Park, D. W.; Kim, I.; Kim, H.; Kang, S. C.; Chi, K.-W. Coordination-Driven Self-Assembly and Anticancer Potency Studies of Ruthenium–Cobalt-Based Heterometallic Rectangles. *Chem. - Eur. J.* **2016**, 22, 16157.

(11) (a) McNeill, S.; Preston, D.; Lewis, J.; Robert, A.; Knerr-Rupp, K.; Graham, D. O.; Wright, J.; Giles, G. I.; Crowley, J. Biologically active [Pd₂L₄]⁴⁺ quadruply-stranded helicates: stability and cytotoxicity. *Dalton Trans.* **2015**, 44, 11129. (b) Preston, D.; McNeill, S. M.; Lewis, J. E. M.; Giles, G. I.; Crowley, J. D. Enhanced kinetic stability of [Pd₂L₄]⁴⁺ cages through ligand substitution. *Dalton Trans.* **2016**, 45, 8050. (c) Ahmedova, A.; Momekova, D.; Yamashina, M.; Shestakova, P.; Momekov, G.; Akita, M.; Yoshizawa, M. Anticancer Potencies of Pt^{II}- and Pd^{II}-linked M₂L₄ Coordination Capsules with Improved Selectivity. *Chem. - Asian J.* **2016**, 11, 474.

(12) (a) Lo, W. K. C.; Huff, G. S.; Preston, D.; McMorran, D. A.; Giles, G. I.; Gordon, K. C.; Crowley, J. D. A Dinuclear Platinum(II) N4Py Complex: An Unexpected Coordination Mode For N4Py. *Inorg. Chem.* **2015**, 54, 6671. (b) Mounir, M.; Lorenzo, J.; Ferrer, M.; Prieto, M. J.; Rossell, O.; Avilés, F. X.; Moreno, V. DNA interaction and antiproliferative behavior of the water soluble platinum supramolecular squares [(en)Pt(N–N)]₄(NO₃)₈ (en = ethylenediamine, N–N = 4,4'-bipyridine or 1,4-bis(4-pyridyl)tetrafluorobenzene. *J. Inorg. Biochem.* **2007**, 101, 660. (c) Bhowmick, S.; Jana, A.; Marri, S. R.; Gupta, P.; Behera, J. N.; Mandal, B. B.; Das, N. Pyrazine based Pt(II) bis-alkynyl organometallic complexes: Synthesis, characterization, and cytotoxic effect on A549 human lung carcinoma cells. *Appl. Organomet. Chem.* **2017**, e3824.

(13) (a) Hannon, M. J.; Painting, C. L.; Jackson, A.; Hamblin, J.; Errington, W. An inexpensive approach to supramolecular architecture. *Chem. Commun.* **1997**, 1807. (b) Oleksi, A.; Blanco, A. G.; Boer, R.; Uson, I.; Aymamí, J.; Rodger, A.; Hannon, M. J.; Coll, M. Molecular recognition of a three-way DNA junction by a metallosupramolecular helicate. *Angew. Chem., Int. Ed.* **2006**, 45, 1227. (c) Hotze, A. C. G.;

Hodges, N. J.; Hayden, R. E.; Sanchez-Cano, C.; Paines, C.; Male, N.; Tse, M.-K.; Bunce, C. M.; Chipman, J. K.; Hannon, M. J. Supramolecular iron cylinder with unprecedented DNA binding is a potent cytostatic and apoptotic agent without exhibiting genotoxicity. *Chem. Biol.* **2008**, *15*, 1258.

(14) (a) Therrien, B.; Süß-Fink, G.; Govindaswamy, P.; Renfrew, A. K.; Dyson, P. J. The “Complex-in-a-Complex” Cations [(acac)₂MCu₆(p-iPrC₆H₄Me)₆(tpt)₂(dhbq)₃]⁶⁺: A Trojan Horse for Cancer Cells. *Angew. Chem., Int. Ed.* **2008**, *47*, 3773. (b) Yan, H.; Süß-Fink, G.; Neels, A.; Stoeckli-Evans, H. Mono-, di- and tetranuclear p-cymeneruthenium complexes containing oxalato ligands. *J. Chem. Soc., Dalton Trans.* **1997**, *0*, 4345. (c) Paul, L. E. H.; Therrien, B.; Furrer, J. Investigation of the Reactivity between a Ruthenium Hexacationic Prism and Biological Ligands. *Inorg. Chem.* **2012**, *51*, 1057. (d) An, S. S.; Kim, I.; Song, Y. H.; Singh, N.; Jeong, Y. J.; Kwon, J. E.; Kim, H.; Cho, Y. M.; Kang, S. C.; Chi, K.-W. Anticancer activities of self-assembled molecular bowls containing a phenanthrene-based donor and Ru(II) acceptors. *Int. J. Nanomed.* **2015**, *10*, 143. (e) Mishra, A.; Jeong, Y. J.; Jo, J.-H.; Kang, S. C.; Kim, H.; Chi, K.-W. Coordination-driven self-assembly and anticancer potency studies of arene–ruthenium-based molecular metalla-rectangles. *Organometallics* **2014**, *33*, 1144.

(15) (a) Kuehl, C. J.; Huang, S. D.; Stang, P. J. *J. Am. Chem. Soc.* **2001**, *123*, 9634. (b) Kryschenko, Y. K.; Seidel, S. R.; Arif, A. M.; Stang, P. J. *J. Am. Chem. Soc.* **2003**, *125*, 5193.

(16) (a) Hall, M. D.; Amjadi, S.; Zhang, M.; Beale, P. J.; Hambley, T. W. The mechanism of action of platinum(IV) complexes in ovarian cancer cell lines. *J. Inorg. Biochem.* **2004**, *98*, 1614. (b) Oldfield, S. P.; Hall, M. D.; Platts, J. A. Calculation of Lipophilicity of a Large, Diverse Dataset of Anticancer Platinum Complexes and the Relation to Cellular Uptake. *J. Med. Chem.* **2007**, *50*, 5227.

(17) Wang, D.; Lippard, S. J. Cellular processing of platinum anticancer drugs. *Nat. Rev. Drug Discovery* **2005**, *4*, 307.

(18) Johnstone, T. C.; Suntharalingam, K.; Lippard, S. J. The Next Generation of Platinum Drugs: Targeted Pt(II) Agents, Nanoparticle Delivery, and Pt(IV) Prodrugs. *Chem. Rev.* **2016**, *116*, 3436.

(19) Attardi, L. D.; de Vries, J. T.; Jacks, T. Activation of the p53-dependent G1 checkpoint response in mouse embryo fibroblasts depends on the specific DNA damage inducer. *Oncogene* **2004**, *23*, 973.

(20) Vermeulen, K.; Berneman, Z. N.; Van Bockstaele, D. R. Cell cycle and apoptosis. *Cell Proliferation* **2003**, *36*, 165.

(21) Vo, V.; Tanthmanatham, O.; Han, H.; Bhowmik, P. K.; Spangelo, B. L. Synthesis of [PtCl₂(4,4'-dialkoxy-2,2'-bipyridine)] complexes and their in vitro anticancer properties. *Metallomics* **2013**, *5*, 973.

(22) Goto, H.; Heemstra, J. M.; Hill, D. J.; Moore, J. S. Single-Site Modifications and Their Effect on the Folding Stability of m-Phenylene Ethynylene Oligomers. *Org. Lett.* **2004**, *6*, 889.

(23) *Apex2, Version 2 User Manual*, M86-E03078, Bruker Analytical X-ray Systems: Madison, WI, 2010.

(24) Sheldrick, G. M. *SHELXTL Program for the Solution of Crystal Structures*; University of Gottingen, Gottingen, Germany, 1993.

(25) (a) Spek, A. L. Structure validation in chemical crystallography. *Acta Crystallogr., Sect. D: Biol. Crystallogr.* **2009**, *65*, 148. (b) van der Sluis, P.; Spek, A. L. BYPASS: an effective method for the refinement of crystal structures containing disordered solvent regions. *Acta Crystallogr., Sect. A: Found. Crystallogr.* **1990**, *46*, 194.